RSC Advances

ROYAL SOCIETY OF CHEMISTRY

www.rsc.org/advances

RSC Advances

RSCPublishing

ARTICLE

Controllable Fabrication of One-dimensional ZnO Nanoarrays and Its Application in Constructing Silver Trap Structures

Yan Bao,[a,b] Yonghui Zhang,[a,b] Jianzhong Ma, [*,a,b] Yanru Zhao [a,b] and Duoduo Wu [a,b]

Cite this: DOI: 10.1039/xoxxoooooox

Received ooth January 2012,
Accepted ooth January 2012

DOI: 10.1039/xoxxoooooox

www.rsc.org/

Large-scale of one-dimensional (1-D) ZnO nanoarrays (NAs) with controllable density and diameter have been successfully fabricated on silver plated aluminium through a simple, low-temperature, two-step strategy. Besides, the silver trap structures constructed based on the prepared 1-D ZnO NAs as the building blocks and its performance in the secondary electron yield suppression were discussed. X-ray diffraction and energy dispersive spectrometer morphologies of the NAs characterized by scanning electron microscopy clarified that, for the 1-D ZnO NAs as-obtained, the density increased and the vertical alignment improved with the concentration of reactants in the aqueous solution. The average diameter of the individual ZnO nanorod varied based both on the density of the NAs and the concentration of the reactants. Increasing the dip-coating times was an effective way to get higher density of ZnO NAs with better vertical alignment under the same conditions. Meanwhile, uniform and dense1-D ZnO NAs with well alignment had been successfully fabricated on PET cloth and stainless steel mesh utilizing this strategy. As for the silver trap structures, there were no obvious differences in the NAs' density before and after the silver trap construction. However, when came to the individual nanorod, the hexagonal surface disappeared while cylindrical one with roughened morphology was obtained at last. Secondary electron yield measurements showed that the silver trap structures exhibited a 30.8% reduction in the secondary electron yield relative to the bare silver plate aluminium, which provided a promising application for this strategy to fabricate desired 1-D ZnO NAs as the building blocks.

Introduction

Nanomaterials (NMs) of one-dimension (1-D), typically including nanotubes (NTs) [1-4], nanowires (NWs) [5-8], nanorods (NRs) [9-12], and nanobelts (NBs) [13-16], have been the focus of intense interest in both academic research and industrial applications in the last two decades. Owing to their one-dimensional structures with high surface-to-volume ratio and rationally designed surface, such NMs do not only exhibit superior electronic, magnetic, optical, chemical and mechanical properties [17-20], but also play an important role as building blocks for other structures [21-23].

ZnO is well-known as the most important multifunctional semiconductor material for its wide band gap (Eg=3.37eV), large excition binding energy (60 meV at room temperature) and excellent chemical and thermal stabilities [24, 25]. 1-D ZnO nanostructures, in particular, have been extensively studied because of its broad applications in electronics, photoelectronics, electrochemical, and electromechanical devices [26-28], such as high-performance nanosensors [29, 30], solar cells [31, 32], nanogenerators [33, 34] and light-emitting diodes [35, 36]. As an amphoteric oxide with an isoelectric point value about 9.5, ZnO can dissolve in either acid or alkaline solution. In addition, there have been various approaches reported to fabricate 1-D ZnO nanostructures with different morphologies. So, it's widely believed that 1-D ZnO nanostructures have a unique advantage in serving as building blocks to construct the fine composite structures.

For the growth of 1-D ZnO structures, vapor-phase processes such as thermal evaporation [37, 38], chemical vapor deposition (CVD) [39, 40], metal organic chemical vapor deposition (MOCVD) [41, 42], and pulsed laser deposition (PLD) [43, 44] are widely used for their simplicity and high-quality products. But most of those approaches either demand vacuum, high temperature, and expensive equipment, or can easily incorporate catalysts or impurities into the ZnO nanostructures, which may limit their potential applications, particularly these requiring for low-cost and large-scale production [28, 45, 46]. Considering these reasons, solution-phase approaches are appealing due to their low cost, less hazardous, high efficiency, and potential for scale-up [47-48]. In addition, the solution growth occurs at a relatively low temperature, and thus compatible with flexible organic substrates [49, 50]. And there are a variety of parameters that can be tuned to effectively control the morphology and further influence the final properties of the product [51].

Among these reported solution-phase approaches, the most widely used is based on the seeded growth of well-oriented ZnO NAs on an existing template layer, where a thin layer of metal Au, Pd and Al served as the catalyst is prepared before the solution growth [47, 52], otherwise a layer of uniform ZnO nanoparticles as the seeds is necessary [53-54]. Li et al. [55] investigated the controllable growth of well-aligned ZnO nanorod arrays on Si substrate via low-temperature wet chemical bath deposition (CBD) method, comprising coating the substrate with ZnO seeds by radiofrequency (RF) magnetron sputtering followed by the growth of ZnO nanorod arrays on the seed-coated substrate in an aqueous solution of zinc ions. Although it provides an effective method to fabricate well-aligned ZnO nanorod arrays with controllable length and diameter, the process is more complicated and often meets the limitation of scale-up production. Tian et al. [56] successfully fabricated micro/nanoscale hierarchical structured ZnO film on stainless steel mesh through a two-step solution approach. This is an excellent work to prepare microscale pore arrays film with photocontrollable water permeation, but it needs 420℃ annealing treatment and more than 15h solution growth which faces limitations in terms of temperature, type of substrates and fabrication cost. Hu et al. [57] synthesized ZnO nanoarray film on FTO substrate at low temperature (＜100℃) by the in situ forced hydrolysis of an anhydrous zinc acetate layer in an aqueous solution, during which the forced hydrolysis of anhydrous zinc acetate was investigated over a wide range of temperatures and concentrations. This offers a precious technique to fabricate optoelectronic devices at low cost and without the use of an expensive catalyst, but the dehydration of zinc acetate dihydrate lasts for 1 day and there was no clear relationship between the controllable growth of ZnO NAs and the experimental conditions.

Herein, we present an easy strategy to fabricate large-scale one dimensional (1-D) ZnO NAs with controllable density and diameter through a cost effective, low-temperature, solution-phase approach. This strategy briefly comprises the preparation of seeded substrate by the facile dip-coating method and growth of 1-D ZnO NAs based on the forced hydrolysis of anhydrous zinc acetate in the heated solution. What makes the difference is that not only the conventional, smooth substrates, but also the reticular substrates are suitable for the controllable fabrication of 1-D ZnO NAs utilizing this strategy. This strategy involves neither the addition of polyethyleneimine (PEI) nor high temperature treatment to fabricate 1-D ZnO NAs with high crystal quality. Thus many promising applications of the prepared 1-D ZnO NAs will be found in a broad range, especially as building blocks to construct fine nano structures for some special purposes. In this paper, the silver trap structures constructed based on the prepared 1-D ZnO NAs and its performance in the secondary electron yield (SEY) suppression will be discussed.

Results and Discussion

Mechanism and Structure

It has been demonstrated that the dehydration of zinc acetate dihydrate occurred under 110W UV irradiation for 1 h and the in situ forced hydrolysis of the anhydrous zinc acetate precursor layer was most important for the subsequent growth of ZnO NAs [57, 59]. In our strategy, the dehydration of zinc acetate dihydrate was taken out by exposing the coated substrate to 300W UV irradiation for 40min. The reactions involved in the solution growth are summarized in the following eqs (1-6)

$$(CH_2)_6N_4 + 6H_2O \longleftrightarrow 6HCHO + 6NH_3 \quad (1)$$

$$NH_3 + H_2O \longleftrightarrow NH_4^+ + OH^- \quad (2)$$

$$Zn^{2+} + 4OH^- \longleftrightarrow [Zn(OH)_4]^{2-} \quad (3)$$

$$[Zn(OH)_4]^{2-} \longleftrightarrow ZnO\downarrow + H_2O + 2OH^- \quad (4)$$

$$Zn(CH_3COO)_2 \longleftrightarrow Zn^{2+} + 2CH_3COO^- \quad \text{(dissolves in the reaction solution)} \quad (5)$$

$$Zn(CH_3COO)_2 + 2OH^- \longleftrightarrow ZnO\downarrow + H_2O + 2CH_3COO^- \quad (6)$$

In the initial stage, HMTA gradually hydrolyzes in the reaction solution and produces OH^- by eq 1 and 2, resulting in the increasing of the pH in the reaction solution. It's well known that anhydrous zinc acetate has low water solubility about 23% at room temperature. When it's in a heated reaction solution having OH^-, anhydrous zinc acetate is more likely to hydrolyze into ZnO grains [59] in situ (in eq 6) by OH^- provided by the decomposition of HMTA rather than dissolving into the reaction solution through eq 5. Therefore, anhydrous zinc acetate on the substrate is changed into ZnO grains on the substrate. Subsequently, the ZnO grains formed here will serve as heterogeneous nucleation and promote the following growth of 1-D ZnO NAs, because heteronucleation is easier and more energetically favorable compared to homogeneous nucleation [28, 60]. While in the bulk reaction solution, the Zn^{2+} from $Zn(NO_3)_2$ $6H_2O$ will coordinate with OH^- by proton transfer, forming the hydroxyl complex of $[Zn(OH)_4]^{2-}$ anion in eq 3, which turns out to be the precursors of ZnO. When the concentration of $[Zn(OH)_4]^{2-}$ in the solution reaches its saturation, the aggregated $[Zn(OH)_4]^{2-}$ will then dehydrate and precipitate out in the form of ZnO via eq 4. The newly formed ZnO prefers to grow into ZnO nanorods based on the heterogeneous nuclear, thus 1-D ZnO NAs are successfully obtained on the substrate.

Figure 1a shows the XRD patterns of the as-obtained 1-D ZnO NAs (in the red line) prepared by employing this new strategy, where the reactants concentration were both fixed at 40mmol/L. Except for the peaks originating from the silver plated substrate (according to the dark line), the diffraction peaks are well consistent with the wurtzite ZnO structure, which can be indexed to a standard spectrum of JCPDS (No. 36-1451). It's noted that the intensity of the 002 peak is much higher than that of other ZnO peaks, indicating the preferential growth of the ZnO NAs along the c-axis direction. The high-magnification SEM image of the as-obtained 1-D ZnO NAs in Figure 1d also proves this point. Moreover, the diameter of ZnO nanorods is uniform. Form the low-magnification SEM image in Figure 1c, the uniform distribution of the as-obtained 1-D ZnO NAs all over the substrate is easily to be distinguished. The corresponding EDS pattern in Figure 1b reveals the presence of Zn and O as the only elementary components with a slight oxygen deficiency (Zn/O atomic ratio≈1:1), while Ag comes from the substrate.

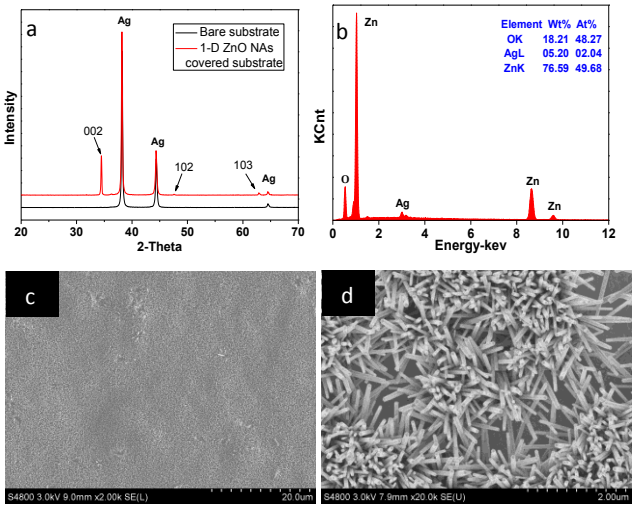

Figure 1 X-ray diffraction patterns (a) , EDS pattern (b) and the corresponding low-magnification (c), high-magnification (d) SEM images of the as-obtained 1-D ZnO NAs on silver plated aluminium substrate

Controllable Fabrication of 1-D ZnO NAs

It's believed that all the reactions listed above are in dynamic equilibrium during the solution growth [28] and can be controlled by adjusting the reaction parameters. Thus, the reactants concentration (the concentration of equimolar $Zn(NO_3)_2$ $6H_2O$ and HMTA) was tuned simultaneously to fabricate 1-D ZnO NAs on the silver plated aluminum by employing this two-step strategy. SEM images of the prepared ZnO NAs were obtained without conductive coating such as Pt and carbon. Figure 2 shows the relationship between the density of the 1-D ZnO NAs and the reactants concentration in the nutrient solution. Overall, the top view images clearly show that the density of the ZnO NAs increases when the reactants concentration increase from 10 mmol/L to 50 mmol/L (in Figure 2a-e). Meanwhile, the morphology of the ZnO NAs changes from the flower-like in discontinuous into the closely packed rod-like. Further increasing the reactants concentration to 100mmol/L, more close-packed ZnO nanorods are obtained as shown in Figure 2f. It's easy to understand that when the reactants concentration is low, for example 10mmol/L, there will be less OH^- generated by the decomposition of HMTA in the heated solution. Thus anhydrous zinc acetate will have less chance to react with OH^- and there will be more anhydrous zinc acetate dissolved into the solution via eq 5. As a result, there are less heterogeneous ZnO nuclear formed as isolated islands on the substrate at the very beginning. The newly formed ZnO in the solution phase will subsequently grow into rod-liked ZnO based on these isolated seeds, while no ZnO nanorods will be obtained on these areas without ZnO seeds because of the large lattice mismatch. Since there is large free outer space for these isolated ZnO seeds to induce the growth of rod-like ZnO in this case, flower-like ZnO NAs with low density are prepared as the final production. In contrast, when the reactants concentration reaches to a sufficient amount, for example 50mmol/L, there will be enough OH^- in the solution to react with anhydrous zinc acetate to form the continuous ZnO seeds on the substrate. Thus the closely packed rod-like ZnO NAs are obtained based on those continuous ZnO seeds as the final product after the solution growth. It's worth noting that the continuous ZnO seeds will provide relatively less free outer space for the growth of each ZnO nanorod [61]. So increasing the reactants concentration not only leads to the increase of the density of the as-obtained ZnO NAs, but also helps to improve the vertical alignment (in Figure 2f) owing to the steric hindrance between the neighbor ZnO nanorods.

According to the previous report, with the increase of reactants concentration, the amount of $[Zn(OH)_4]^{2-}$ produced from nutrient solution will increase correspondingly, which will increase the speed of growth during ZnO synthesis. These processes are endothermic and will hinder ZnO nanorod arrays growth along the [0001] direction. On the other hand, when the reactants concentration reaches to a sufficient amount, ZnO seeds hydrolyzed by anhydrous zinc acetate on the substrate do not depend on the reactants concentration. That's why increasing the reactants concentration from 50mmol/L to 100mmol/L resulted in the increasing of the average diameter of the as-obtained ZnO nanorods from about 60nm to 130nm, but the density of the NAs remained similar in this case.

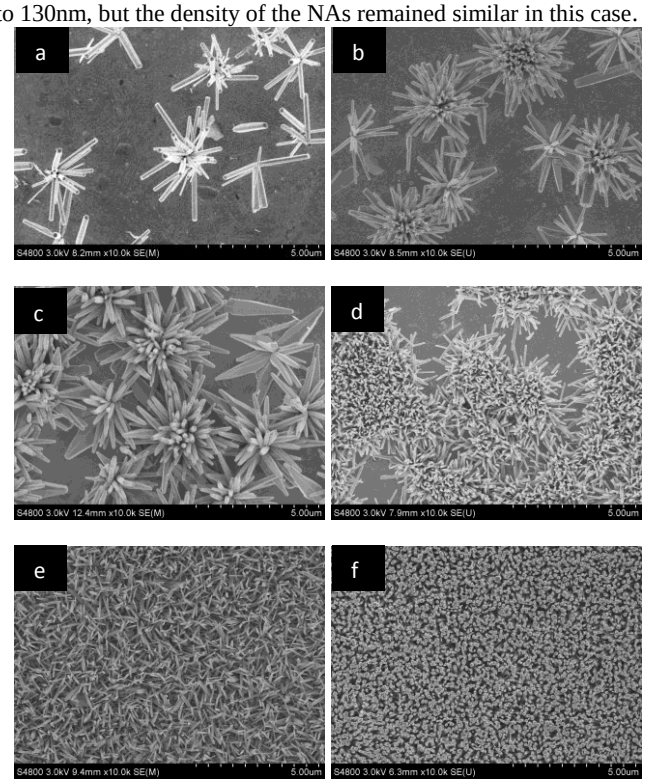

Figure 2 SEM images of 1-D ZnO NAs grown in (a) 10mmol/L, (b) 20mmol/L, (c) 30mmol/L, (d) 40mmol/L, (e) 50mmol/L and 100mmol/L (f) reactants solution

In general, the in situ forced hydrolysis of anhydrous zinc acetate plays the most important role in the final density of the as-grown ZnO NAs. Increasing the reactants concentration is an effective way to improve the forced hydrolysis of anhydrous zinc acetate and heteronucleation, which derives the growth of 1-D ZnO NAs with high density. Meanwhile, for the ZnO NAs with high density, the vertical alignment is improved and the average diameter can be tuned by adjusting the reactants concentration during the synthesis process.

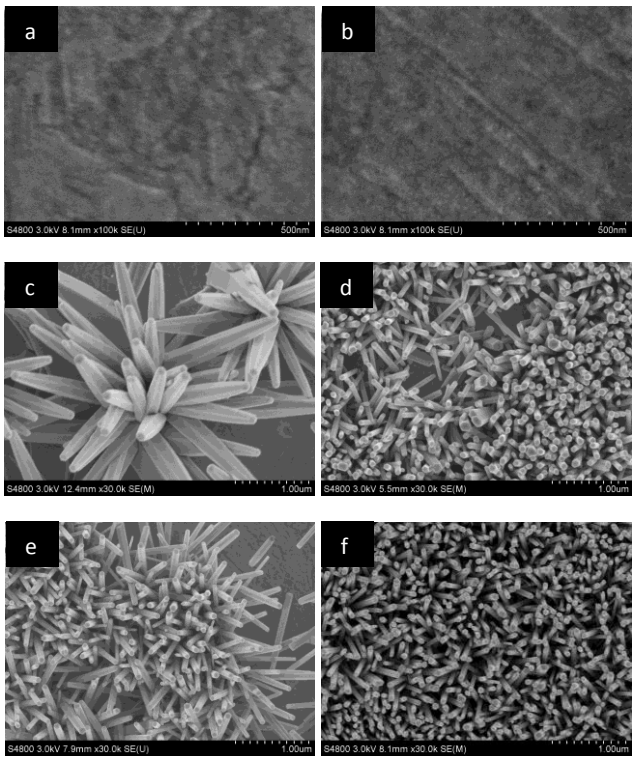

Figure 3 SEM images of seeded substrate with three (a), five (b) times dip-coating and 1-D ZnO NAs grown in 30mmol/L (b), 40mmol/L (c) reactants solution based on the seeded substrate with three times dip-coating and in 30mmol/L (e), 40mmol/L (f) reactants solution based on the seeded substrate with five times dip-coating

As mentioned above, the forced hydrolysis of anhydrous zinc acetate is so important for the heteronucleation that we then conducted the dip-coating step for five times to prepare the seeded substrate. But there showed no clear differences in the surface micrographs between the seeded substrate with three times and five times dip-coating (in Figure 3a, b). As for the 1-D ZnO NAs grown on these substrates in both 30mmol/L and 40mmol/L reactants solution, it's obvious that the 1-D ZnO NAs grown on the substrate with five times dip-coating (in Figure 3d, f) has higher density and better vertical alignment, compared to those grown on the substrate with three times dip-coating (in Figure 3c, e). It's supposed that increasing the dip-coating times leads to the increasing of the layer thickness of anhydrous zinc acetate, which will further influence the forced hydrolysis of anhydrous zinc acetate. That's when increasing the dip-coating times, there will be more opportunities for the forced hydrolysis of anhydrous zinc acetate into the denser ZnO nucleation sites on the substrate. And the denser ZnO nucleation sites will then induce the growth of denser ZnO NAs with improved vertical alignment due to the steric hindrance. Also it's noted that the ZnO nanorods based on five times dip-coating have smaller diameters than those based on three times dip-coating either grown in 30mmol/L or in 40mmol/L reactants solution. For example, the ZnO nanorods based on five times dip-coating have an average diameter about 50nm, smaller than those based on three times with the average diameter about 70nm when grown in 40mmol/L reactants solution. This is mostly because the amount of Zn^{2+} is constant in the reactants solution, and the denser nucleation sites will reasonably derive in ZnO nanorods with smaller diameter in the same reactants solution.

In a word, either increasing the dip-coating times or increasing the reactants concentration is beneficial for the uniform distribution of ZnO nucleation sites on the substrate at the very beginning, which will then help to grow 1-D ZnO NAs with higher density and better vertical alignment. So 1-D ZnO NAs with desired density and diameter can be fabricated utilizing this new strategy, by adjusting the parameters during the fabrication process.

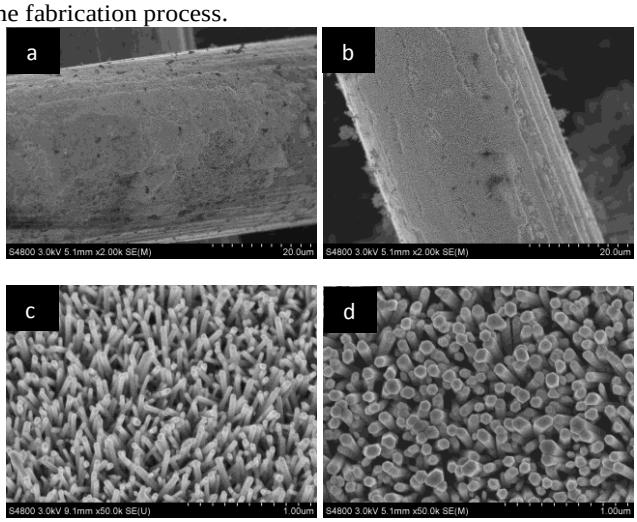

Figure 4 SEM images of 1-D ZnO NAs grown on PET (a, b) and stainless steel mesh (c, d)

To provide additional information that this strategy can be employed to fabricate 1-D ZnO NAs on different substrates, PET cloth and stainless steel mesh were selected to carry out the fabrication process, during which the temperature was kept at 95℃ and the solution growth lasted for 4h. Figure 4 shows the SEM images of ZnO NAs grown on PET cloth and stainless steel mesh utilizing this strategy with the reactants concentration fixed at 40mmol/L. It's clear that both the PET cloth and stainless steel mesh are covered with a uniform and dense film of ZnO nanorods. The as-prepared nanorods are well faceted with a typical diameter of about 50nm and 95nm, respectively, in this given growth conditions.

Texture Surface and SEY Suppression of Silver Trap Structures Based on 1-D ZnO NAs.

SEY, which represents the number of emitted secondary electrons per primary incident electron, is usually used to characterize the secondary electron emission (SEE) properties of a material. In the quest of suppressing multipactor discharge and electron cloud effects caused by SEE, to fabricate satellites and accelerators in high performance, several methods are under intense study to lower the SEY [63]. One of the most effective methods is to manufacture deeply roughened surface as trap structures, in which the secondary electrons excited by primary electrons can be efficiently trapped through the constant collisions inside the trap structures. Given that silver is one of the best conductive metals in the world, constructing silver trap structures is considered as a most promising approach to effectively suppress SEY.

The construction of silver trap structures was conducted utilizing the 1-D ZnO NAs shown in figure 3d as the building blocks. SEM images of nanoarrays obtained after electrodeposition of silver and the final silver trap structures are shown in figure 5a and 5b, respectively. There shows no obvious differences in the nanoarrays density when compared to that in figure 3d, but the average diameter increased a little to about 65nm after the deposition process of silver (in figure 5a) and then decreased slightly back to 50nm because of the ZnO etched by acid (in figure 5b). For the morphology of each nanorod, the original hexagonal contours of ZnO turned into cylindrical shape after the deposition of silver (see the upper right inset in figure 5a), while further treatment in acid solution resulted in a rougher surface (see the upper right inset in figure 5b).

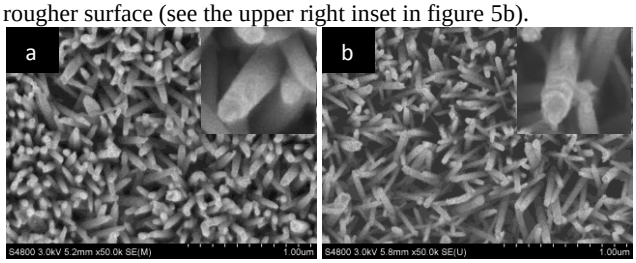

Figure 5 SEM images of the obtained nanoarrays after electrodeposition of silver (a) and the silver trap structures (b)

Figure 6a shows the XRD patterns of the obtained nanoarrays after electrodeposition of silver (SAM 1, in the red line) and the final silver trap structures (SAM 2, in the blue line). It's well defined that the intensity of the typical peaks originating from 1-D ZnO NAs decreased much after the etching treatment in acid solution, supporting that most of the building blocks, namely 1-D ZnO NAs, have been removed and the silver trap structures have been successively constructed as the final products. As for the SEY measurement, each sample has been tested for three different positions to calculate the average and the results are shown in figure 6b. First, we measured the SEY of the bare substrate (in the dark line), which had a maximum SEY of about 2.24. For the substrate covered with silver trap structures, the maximum SEY was about 1.55, indicating a 30.8% reduction relative to the original sample.

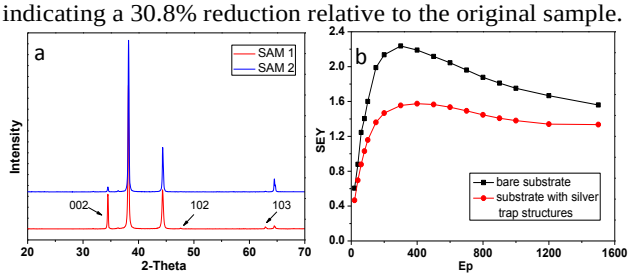

Figure 6 (a) XRD patterns of the substrate covered with 1-D ZnO nanoarrays after electrodeposition of silver (SAM 1) and silver trap structures (SAM 2), (b) the measured SEY characteristics of the silver trap structures

Since the SEY of a roughened surface can be sharply suppressed by increasing the aspect ratio of the micro-pores and the surface porosity of the metal plate [64]. And it has been concluded above that1-D ZnO NAs with desired density and diameter can be successively fabricated by employing this two-step strategy. So it's very promising for the SEY to be much more suppressed with this new strategy to fabricate 1-D ZnO NAs with proper density and diameter, which will serve as the building blocks to construct the optimal silver trap structures here.

Experimental Section

Materials

All the reagents used in the experiment were analytical grade and utilized without any further purification. Zinc nitrate hexahydrate ($Zn(NO_3)_2 \cdot 6H_2O$, ≥99.0%) and hexamethylenetetramine ($C_6H_{12}N_4$, 99.0%) were purchased from Tianjin Chemical Reagent Factory. Silver nitrate ($AgNO_3$, 99.8%) was obtained from Shanghai Shiyi Chemicals Reagent Co., Ltd. Zinc acetate dehydrate ($Zn(CH_3COO)_2 \cdot 2H_2O$, ≥99.0%), acetone ($C_3H_6O$, ≥99.5%) and anhydrous ethanol (C_2H_5OH, ≥99.7%) were provided by Tianjin Hongyan Chemical Reagent Factory. Virtually any substrate is suitable as long as a uniform film of seeds layer can be prepared on it. In this paper, commercially available silver plated aluminium, PET cloth and stainless steel mesh were chosen as substrate.

Fabrication of 1-D ZnO NAs

To grow 1-D ZnO NAs on the substrate, a simple two-step strategy was employed as shown in Figure 7. First, the substrate (2cm×1.5cm) was cleaned by successive sonication in soap, deionized water, acetone and anhydrous ethanol. Then it was coated with a thin film of zinc acetate dihydrate (Figure 7b), by dip-coating in a 0.01mol/L zinc acetate dihydrate-anhydrous ethanol solution and drying in air at 65℃. This dip-coating step was repeated another twice to ensure the uniform coverage of zinc acetate dihydrate. Subsequently, the coated substrate was exposed to UV radiation in the air for 40min using a 300W UV lamp (ULTRA VITALUX, OSRAM) and the work distance was maintained at 5cm. This radiation process was carried out for the dehydration of zinc acetate dihydrate to form the seeds layer (Figure 7c) on the substrate that would induce the following growth of ZnO NAs on the substrate.

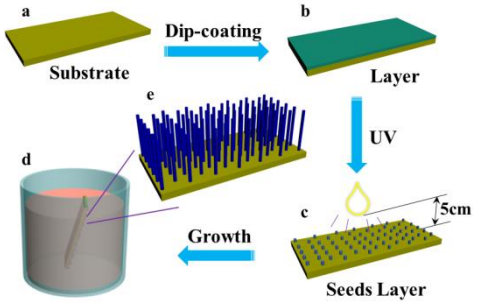

Figure 7 schematic diagram of solution synthesis of 1-D ZnO NAs: (a) cleaned substrate, (b) dip-coated substrate with zinc acetate dihydrate, (c) seeded substrate fabricated by exposing the zinc acetate dihydrate layer to UV light, (d) solution growth of 1-D ZnO NAs on the seeded substrate, (e) 1-D ZnO NAs as-obtained on the seeded substrate.

For the solution growth of 1-D ZnO NAs on the substrate, the seeded substrate was immersed upside down with an angle in 50mL

aqueous solution (Figure 7d) that contained a fixed concentration (0.01~0.10mol/L) of equimolar $Zn(NO_3)_2$ $6H_2O$ and hexamethylenetetramine (HMTA). The solution was kept at 95 ℃ for 4 hours in a thermostatically regulated water bath. Finally, the samples (Figure 7e) were removed from the solution, rinsed with deionized water and dried in the air for further characterization.

Construction of sliver trap structures

Construction of sliver trap structures based on the prepared 1-D ZnO NAs was carried out in a two-electrode configuration at room temperature, in which the 1-D ZnO NAs covered silver plated aluminium and equal-area sliver foil served as the working electrode and counter electrode, respectively (see Figure 8). The electrolyte solution was prepared by dissolving 0.01mol/L $AgNO_3$ into anhydrous ethanol-deionized water with the volume ratio about 4:1. The plane distance between the two electrodes was kept at 2.5cm during the whole process. The applied potential supplied by DC power (PS-303D, LONGWEI) and duration were 0.8V and 20min, respectively. After an interval of 10min, the deposition was continued for another 20min. Subsequently, the working electrode was rinsed with deionized water several times and immersed in 0.001mol/L HCl to remove the ZnO. Finally, the sample was again rinsed with deionized water several times and dried in the air for further characterization.

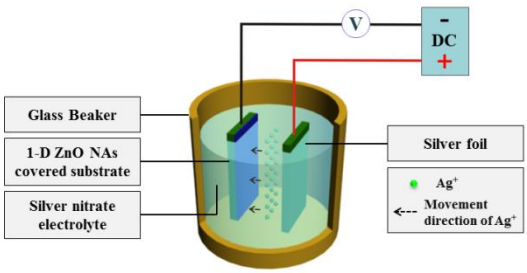

Figure 8 schematic diagram of construction of sliver trap structures based on the prepared 1-D ZnO NAs

Characterization

The morphology and composition of the as-prepared 1-D ZnO NAs was examined by scanning electron microscopy (SEM, HITACHI S-4800 operated at 3.0 kV) combined with energy dispersive spectroscopy (EDS). X-ray diffraction (XRD) patterns were obtained on a Rigaku D/max diffractometer with Cu K_α radiation (40kV, 40mA) at a scan rate of 2 °/min to identify the crystalline phase and orientation of the samples. The SEY of the constructed silver trap structures was measured via the conventional sample-current method [58]. With an electron beam focusing on the sample, when biased at -20 V, the measured sample-to-ground current I_S was taken to be the total beam current except for the secondarily emitted current. When 500 V was applied to the sample, the emitted electrons would then be retained by the sample and the resulting sample-to-ground current is taken to be the total beam current, I_P. Thus, the total SEY is taken to be:

$$\delta = (I_p - I_s)/ I_p$$

Conclusion

In summary, 1-D ZnO NAs with controllable density and diameter can be realized by adjusting the dip-coating times and reactants concentration utilizing this two-step strategy. Nearly any substrate is suitable for the growth of 1-D ZnO NAs as long as a uniform film of seeds layer can be prepared on it. For example, when repeating the dip-coating step for five times and fixing the reactants concentration at 40mM, a uniform and dense film of ZnO NAs can be obtained on silver plated aluminium, PET cloth and stainless steel mesh. This strategy features simplicity, reproducibility, cost-efficiency and suitability for large-scale production. We believe that this two-step strategy has a wide potential application in fabricating 1-D ZnO NAs as building blocks to construct fine nano structures for some special purposes. Notably, when employing the 1-D ZnO NAs prepared in 40mM reactants concentration to construct silver trap structures, the structures shows a 30.8% reduction in the SEY relative to the bare silver plate. And it's very promising for the SEY to be much more suppressed by optimizing the building blocks' structure with this new strategy. Also, this strategy can be used to fabricate 1-D ZnO NAs on the stainless steel mesh or porous ceramic substrate for the photocatalytic degradation of organic pollutants and adsorption of heavy metal ions in the wastewater. In addition, this two-step strategy will find potential use in the surface functional modification in many other areas to fabricate portable and foldable devices in the near future.

Acknowledgements

This research was supported by the National Natural Science Foundation (21376145), Program for New century excellent talents in university (NCET-13-0885) and Key Scientific Research Group of Shaanxi Province (2013KCT-08).

Notes and references

[a] College of Resources and Environment, Shaanxi University of Science & Technology, Xi'an 710021, China.
[b] Shaanxi Research Institute of Agricultural Products Processing Technology, Xi'an 710021, China.
* The corresponding author. E-mail: Majz@sust.edu.cn.

1 Jacobs C B, Peairs M J and Venton B J, Anal. Chim. Acta., 2010, **662(2)**, 105.
2 Yang X F, Tang H and Cao K S, et al. J. Mater. Chem., 2011, **21**, 6122.
3 Xiao F X, ACS Appl. Mater. Interfaces, 2012, **4(12)**, 7055.
4 Yang P H, Wang K and Liang Z W, et al. Nanoscale, 2012, **4(18)**, 5755.
5 Li Z, Gao F and Kang W J, et al. Mater. Lett., 2013, **97**, 52.
6 Zhao Y G, Yan X Q and Kang Z, et al. Mikrochim. Acta, 2013, **180(9-10)**: 759.
7 Lu S N, Qi J J and Wang Z Z, et al. RSC Adv., 2013, **3(42)**, 19375.
8 Pradel K C, Wu W Z and Zhou Y S, et al. Nano Lett., 2013, **13(6)**, 2647.
9 Valls I G, Cantu M L, Energy Environ. Sci., 2010, **3(6)**, 789.

10 Yi J, Lee J M and Park W II, Sens. Actuators, B, 2011, **155(1)**, 264.
11 Huang X H, Zhang C and Tay C B, et al. Appl. Phys. Lett., 2013, **102(11)**, 111106.
12 Cheng C W, Sie E J and Liu B, et al. Appl. Phys. Lett., 2010, **96(7)**, 071107.
13 Yang Y, Qi J J and Guo W, et al. Phys. Chem. Chem. Phys., 2010, **12**, 12415.
14 Xing G Z, Fang X S and Zhang Z, et al. Nanotechnology, 2010, **21(25)**, 255701.
15 Yang Y, Guo W and Qi J J, et al. Appl. Phys. Lett., 2010, **97**, 223113.
16 Monmeni K, Odegard G M and Yassar R S, Acta Mater., 2012, **60(13-14)**, 5117.
17 Yu M, Long Y Z and Sun B, et al. Nanoscale, 2012, **4(9)**, 2783.
18 Lu X F, Zhang W J and Wang C, et al. Prog. Polym. Sci., 2010, **36(5)**, 671.
19 Barth S, Ramirez F H and Holmes J D, et al. Prog. Mater. Sci., 2010, **55(6)**, 563.
20 Fang X S, Hu L F and Ye C H, et al. Pure Appl. Chem., 2010, **82(11)**, 2185.
21 Liang H W, Liu S and Yu S H. Adv. Mater., 2010, **22(35)**, 3925.
22 Baca A J, Ahn J H and Sun Y G, et al. Angew. Chem. Int. Edit., 2008, 47(30), 5524-5542.
23 Yang P H, Xiao X and Li Y Z, et al. ACS Nano, 2013, **7(3)**, 2616.
24 Gu Z J, Paranthaman M P and Xu J, et al. ACS Nano, 2009, **3(2)**, 273.
25 Liu J P，Huang X T and Li Y Y, et al. J. Phys. Chem. C, 2007, **111(13)**:4990.
26 Wen B M, Huang Y Z and Boland J J. J. Phys. Chem. C, 2008, **112(1)**, 106.
27 Xu X B, Wu M and Asoro M, et al. Cryst. Growth Des., 2012, **12**, 4829.
28 Xu S and Wang Z L. Nano Res., 2011, **4(11)**, 1013.
29 Qi G C, Zhao S Z and Yuan Z H. Sens. Actuators, B, 2013, **184**, 143.
30 Pan C F, Yu R M and, Niu S M, et al. ACS Nano, 2013, **7(2)**, 1803.
31 Yang Y, Guo W X and Zhang Y, et al. Nano Lett., 2011, **11(11)**, 4812.
32 Fan J D, Hao Y and Munuera C. et al. J. Phys. Chem. C, 2013, **117(32)**, 16349.
33 Yang Y, Pradel K C and Jing Q S, et al. ACS Nano, 2012, **6(8)**, 6984.
34 Chen C Y, Huang J H and Song J H, et al. ACS Nano, 2011, **5(8)**, 6707.
35 Yang Q, Liu Y and Pan C F, et al. Nano Lett., 2013, **13(2)**, 607.
36 Zhang Y, Ge L and Li M, et al. Chem. Commun., 2014, **50(12)**, 1417.
37 Pan Z W, Dai Z R and Wang Z L, Science, 2001, **291(5510)**, 1947.
38 Lee J S, Islam M S and Kim S. J. Sens. Actuators, B, 2007, **126**: 73.
39 Shen J B, Zhuang H Z and Wang D X, et al. Cryst. Growth Des., 2009, **9(5)**, 2187.
40 Yan Y, Zhou L and Han Y, et al. J. Phys. Chem. C, 2010, **114(9)**, 3932.
41 Park W I, Kim D H and Jung S W. et al. Appl. Phys. Lett., 2002, **80(22)**, 4232.
42 Barreca D, Bekermann D and Comini E, et al. J. Sens. Actuators, B, 2010, **149(1)**, 1.
43 Hong J I, Bae J and Wang Z L, et al. Nanotechnology, 2009, **20(8)**, 085609.
44 Shen Y, Hong J I and Peng Z C, et al. J. Phys. Chem. C, 2010, **114(49)**, 21277.
45 Wang Z L, Mater. Sci. Eng., R, 2009, **64(3-4)**, 33.
46 Weintraub B, Zhou Z Z and Li Y H, et al. J. Nanoscale, 2010, **2(9)**: 1573.
47 Tian J H, Hu J and Li S S, et al. Nanotechnology, 2011, **22**, 245601.
48 Tang Y, Chen J and Greiner D, et al. J. Phys. Chem. C, 2011, **115(13)**, 5239.
49 Liu T Y, Liao H C and Lin C C, et al. Langmuir, 2006, **22(13)**, 5804.
50 Qin Y, Yang R S and Wang Z L, J. Phys. Chem. C, 2008, **112(48)**, 18734.
51 Xu S, Adiga N and Ba S, et al. ACS Nano, 2009, **3(7)**, 1803.
52 Xu S, Lao C S and Weintraub B, et al. J. Mater. Res., 2008, **23(8)**, 2072.
53 Li Q C, Kumar V and Li Y, et al. J. Chem. Mater., 2005, **17(5)**, 1001.
54 Hu Y F, Zhang Y and Xu C, et al. Nano Lett., 2011, **11(6)**, 2572.
55 Li Q, Bian J and Sun J, et al. Appl. Surf. Sci., 2010, **256(6)**, 1698.
56 Tian D, Zhang X and Zhai J, et al. Langmuir, 2011, **27(7)**, 4265.
57 Hu X L, Masuda Y and Ohji T, et al. J. Cryst. Growth, 2009, **311(3)**, 597.
58 Ye M, He Y N and Hu S G, et al. J. Appl. Phys., 2013, **114(10)**, 104905.
59 Hu X L, Masuda Y and Ohji T, et al. Langmuir, 2008, **24(14)**, 7614.
60 Vayssieres L, Keis K and Lindquist S E, et al. J. Phys. Chem. B, 2001, **105(17)**, 3350.
61 Liang J K, Su H L and Kuo C L, et al. Electrochim. Acta, 2014, **125**, 124.
62 Zhang H, Yang D and Ji Y, et al. J. Phys. Chem. B, 2004, **108(13)**, 3955.
63 Pivi M, King F K and Kirby R E, et al. J. Appl. Phys., 2008, **104(10)**, 104904.
64 Ye M, He Y N and Hu S G, et al. J. Appl. Phys., 2013, **113(7)**, 074904.